Talanta 219 (2020) 121342

Contents lists available at ScienceDirect

Talanta

journal homepage: www.elsevier.com/locate/talanta

# A metal-organic framework/aptamer system as a fluorescent biosensor for determination of aflatoxin B1 in food samples

Yongmei Jia [a], Guohua Zhou [a,*], Xudong Wang [b,**], Yingzi Zhang [c], Zhiguo Li [a], Peilian Liu [a], Biao Yu [a], Jun Zhang [a]

[a] School of Chemistry and Chemical Engineering, Lingnan Normal University, Zhanjiang, 524048, China
[b] National Center for Nanoscience and Technology, Beijing, 100190, China
[c] Institution of Supervision and Inspection Product Quality of Guizhou Province, Guiyang, 550016, China

ARTICLE INFO

*Keywords:*
Aflatoxin B1
UiO-66-$NH_2$
Fluorescence
Aptamer

ABSTRACT

The demand of simple, sensitive, selective and reliable assay for aflatoxin B1 (AFB1) detection is ubiquitous in food safety, due to its high toxic. Herein, a novel fluorescent aptasensor using metal-organic frameworks (UiO-66-$NH_2$) and TAMRA label aptamer as sensing platform for AFB1 detection was developed. The TAMRA aptamer adsorbed on the surface of UiO-66-$NH_2$ via van der Waals force and its fluorescence was quenched for the charge transfer from fluorescence dye TAMRA to metal ions of UiO-66-$NH_2$. After introducing AFB1 to the system, the TAMRA aptamer binded to AFB1 and formed TAMRA aptamer/AFB1complex, making its conformation change and resulting in fluorescence recovery. Thus, the quantity of AFB1 could be analyzed according to the fluorescence signal change. Under optimize experimental conditions, the assay exhibited high sensitivity toward AFB1 in range of 0–180 ng $mL^{-1}$ with low limit of detection of 0.35 ng $mL^{-1}$ and good specificity against other toxins. Moreover, the aptamer/metal-organic frameworks sensing platform could be utilized to determine AFB1 content in food samples such as corn, rice and milk. It provided a reasonable method for other mycotoxin detection by changing the sequence of aptamer.

## 1. Introduction

Aflatoxins (Aspergillus flavus toxins) are secondary metabolites produced by Aspergillus flavus and Aspergillus parasiticus, which exist in various kinds of agricultural products including corn, peanuts and grains [1]. Among these aflatoxins, aflatoxins B1 (AFB1) is considered as the most toxic one for it could enter into human beings or other animals through food chain and lead to liver cirrhosis or necrosis [2–4]. Thus, developing sensitive and selective analytical assays for AFB1 detection is vitally important. In the last years, a great deal of studies have been performed on sensitive and quantitative determination of AFB1 in foods and agricultural products. Conventional AFB1 detection methods included liquid chromatography (HPLC), thin-layer chromatography (TLC), gas chromatography (GC) and mass spectrometry (MS) [5,6], in which the assays need skilled operators, time-consuming sample pretreatments as well as expensive instrumentation [7,8]. Due to these disadvantages, several other immunoassays based on the specific combination of antigen and antibody had been developed to monitor the AFB1 content [9,10]. While, these assays need difficult preparation and high cost of antibodies, which limited their widespread application.

Aptamers are a type of DNA or RNA sequence that are selected via in vitro selection process by exponential enrichment (SELEX). They could specifically bind to the corresponding target with high affinity and selectivity, have captured tremendous attention [11]. Compared with antibodies, they own a variety of advantages including flexible synthesis and labelling, easy storage, high stability and good binding affinity. Different types of aptamer based biosensors such as surface plasmon resonance, quartz crystal microbalance (QCM), silicon-based light addressable potentiometric sensor and bead array counter biosensor had been constructed to analyze various targets such as metal ions, small molecules, proteins, cells and microorganisms [12,13]. These aptamer bisosensors exhibited high sensitive for targets detection in buffer, while unspecific binding in complex samples. With the increasing awareness of the risk arising from food contamination, aptamers were employed to

* Corresponding author.,
** Corresponding author.
*E-mail addresses:* ghzhou@lingnan.edu.cn (G. Zhou), wangxd2019@nanoctr.cn (X. Wang).

https://doi.org/10.1016/j.talanta.2020.121342
Received 26 March 2020; Received in revised form 22 June 2020; Accepted 26 June 2020
Available online 9 July 2020

detect targets in food samples including brucella melitensis, staphylococcus aureus and toxins [14]. Thus, it was an urgent thing to explore a new type of aptamer based biosensor for target detection in food samples with high sensitive and specific.

There were reports had been established to detect AFB1 by using AFB1 aptamer such as fluorescent [15–18], colorimetric [19–22], electrochemical [23–27] and surface-enhanced raman scattering aptamer sensors [28]. Among them, the fluorescent aptamer sensors possess the advantages of ease of operation, high sensitivity and in situ imaging properties [29,30]. In addition, they were extensively used for AFB1 detection. Nevertheless, most of them need the aptamers labeled with fluorophores and quenchers. The detection of AFB1 was realized by tuning the distance of fluorophore and quencher. Although these fluorescent aptamer sensors had been utilized to monitor AFB1 in a wide range, fluorophore-quencher pair still required careful selection to ensure optimum efficiency. Thus increasing the difficult of aptamers synthesis, which was the major shortcoming.

To circumvent such drawbacks, nanomaterials had been employed to fluorescent aptamer sensors for AFB1 detection including graphene oxide [31], transition metal dichalcogenides [32], humic acid [33] and Au nanoparticles [34]. They were capable of quenching the fluorescence of various fluorophore and acted as quenchers to improve the signal-to-noise ratio. While, these nanomaterials were subjected to expensive, sophisticate, time-consuming as well as strict prepare progress. Additionally, the uneven size of the above nanomaterials resulted in interactions between nanomaterials and aptamers were easy effected by reaction condition [35,36]. Recently, metal-organic frameworks (MOFs) which were constructed by self-assembling of metal ions and organic ligands had been introduced to biosensors owing to its flexible porosity, high surface area, tunable pore sizes, high thermal and chemical stability [37–39]. Furthermore, they could be intrinsically biodegradable after completing an intended task. To the best of our knowledge, there were few reports on using MOFs as sensing platform for analyzing mycotoxin in food samples.

Inspired by these findings, we established an AFB1-aptamer/MOFs sensing paltform to monitor AFB1 in food samples, such as corn, rice and milk. AFB1 aptamer labeled with the fluorescence dye TAMRA. UiO-66-$NH_2$ was selected as the MOFs nanomaterial. The TAMRA aptamer adsorbed on the surface of UiO-66-$NH_2$ via van der Waals force and its fluorescence was quenched for the charge transfer from fluorescence dye TAMRA to metal ions of UiO-66-$NH_2$ [40,41]. In the presence of target AFB1, TAMRA aptamer changed into internal loop structures and detached from UiO-66-$NH_2$ surface for the decrease adsorption affinity, leading to fluorescence recovery. The assay exhibited a good linear relationship in range from 0 to 0.5 ng $mL^{-1}$ and 1.5–3.0 ng $mL^{-1}$, the low detection limit was 0.35 ng $mL^{-1}$. More importantly, the designed sensing platform was capable of detecting AFB1 in real food samples including corn, rice and milk. The result illustrated that the proposed fluorescent aptasensor provides a reliable tool for mycotoxins determination in food samples.

## 2. Materials and methods

### 2.1. Materials

Aflatoxin B1 (AFB1), Zearalenone (ZEN) and Ochratoxin A (OTA) were purchased from Sigma-Aldrich (USA). UiO-66-$NH_2$ was obtained from Aladdin Reagent Co., Ltd (Shanghai, China). Other chemical reagents were at analytical grade and purchased from Sinopharm Chemical Reagent Co., Ltd. (Shanghai, China). The samples of corn, milk and rice were bought from local supermarket (Zhanjiang, China). The aptamers were synthesized by Shanghai Sangon Biotechnology Co., Ltd (Shanghai, China) and purified with HPLC. The sequence of the aptamers was listed as follows:

TAMRA aptamer (from 5′ to 3'): TARMA-GTT GGG CAC GTG TTG TCT CTC TGT GTC TCG TGC CCT TCG CTA GGC CCA CA.

### 2.2. Apparatus

The fluorescence emission spectra was recorded by Cary Eclipse F-4500 (Agilent Technologies, USA). The HPLC data was measured using an Agilent 1260. The UV–vis absorption spectra was recorded by UV-3600 (Shimadzu, Japan). The nanoparticle size was tested by 90 Plus Zeta (Brookhaven Instruments Corporation, USA).

### 2.3. Optimization of MOF concentration

3.8 mg UiO-66-$NH_2$ samples were dispersed in 400 mL $H_2O$ by sonication to form 9.5 μg $mL^{-1}$ suspension. Then different concentrations of UiO-66-$NH_2$ from 6.79 × $10^{-3}$ to 339.00 × $10^{-3}$ μg $mL^{-1}$ and TAMRA aptamer (37.5 nmol $L^{-1}$) were added to Tris-HCl buffer (10 mM Tris, 120 mM NaCl, 5 mM KCl, pH 7.21) giving the final reaction volume of 70 μL. After incubating 30 min with 300 rpm shake at 30 °C, their fluorescence intensity were tested. The samples were excited at 560 nm while the emission spectra were collected at wavelength ranging from 570 to 700 nm at room temperature. Each experiment was performed three times.

### 2.4. Sensitivity of the sensing platform

The TAMRA aptamer (37.5 nmol $L^{-1}$), UiO-66-$NH_2$ (0.2 μg $mL^{-1}$) suspension and different concentrations of AFB1 from 0.005 to 180 ng $mL^{-1}$ were mixed in Tris-HCl buffer (10 mM Tris, 120 mM NaCl, 5 mM KCl, pH 7.21). After samples incubated for 55 min at 37 °C, their fluorescence intensity were tested. The samples were excited at 560 nm while the emission spectra collects at wavelength ranging from 570 to 700 nm at room temperature. Each experiment was performed three times.

### 2.5. Specificity of the sensing platform

The specificity of the assay to AFB1 was studied using the mycotoxins, ochratoxin A (OTA) and zearalenone (ZEN) as comparison. The TAMRA aptamer (37.5 nmol $L^{-1}$), UiO-66-$NH_2$ (0.2 μg $mL^{-1}$) suspension and AFB1 or mycotoxins (OTA or ZEN) were added to Tris-HCl buffer (10 mM Tris, 120 mM NaCl, 5 mM KCl, pH 7.21). The final concentration of OTA or ZEN was 210 ng $mL^{-1}$. The final concentration of AFB1 was 70 ng $mL^{-1}$. After incubating for 55 min at 37 °C. Their fluorescence intensity were measured.

### 2.6. Quantitative measurement of AFB1 in food samples

The pretreatment of milk, corn and rice samples was according to our previous report [42]. Briefly, the samples were shaken in 4 mL methanol-water (70:30, v/v) solution for 1 h at 30 °C, and then the extracts were centrifuged at 12,000 rpm for 10 min. Then, the extracts filter through a disposable syringe filter until the solution was clear. Last, the filtrate was diluted in 3 mL Tris-HCl buffer. Two different concentrations of AFB1 were spiked into the extracts to obtain standard samples, then detected by HPLC and our assay in this work.

## 3. Results and discussion

### 3.1. The principle of the designed aptasensor

Here, we developed an AFB1-aptamer/MOFs platform for AFB1 detection composed of AFB1 aptamer labeled with fluorophores (TAMRA) and conjugated with MOFs (UiO-66-$NH_2$). The TAMRA aptamer adsorbed on the surface of UiO-66-$NH_2$ via the van der Waals force, which decrease the fluorescence intensity of the dyes TAMRA for the charge transfer from fluorescence dye TAMRA to metal ions of UiO-66-$NH_2$ [43,44]. In the presence of target AFB1, it incubated with TAMRA aptamer, making the TAMRA aptamer change into internal loop

structures and detaching from the surface of UiO-66-$NH_2$. Thus, the flluorescence emission was recovered for it obstructs the energy transfer between the fluorescence dye TAMRA and UiO-66-$NH_2$ (Scheme 1). And the quantity of AFB1 could be analyzed by monitoring TAMRA aptamer fluorescence intensity change.

### 3.2. Optimization of MOF concentration

Since UiO-66-$NH_2$ acted as a quencher in the sensing platform, it was therefore vital to determine the optimum amount of UiO-66-$NH_2$ to be adopted in the assay. As shown in Fig. S1, the fluorescence highly enhanced with increasing the concentration of TAMRA aptamer. To obtain a desirable fluorescence response, 37.5 nmol $L^{-1}$ of TAMRA aptamer was choose for the subsequent experiments. Too much UiO-66-$NH_2$ in the system might lead to low fluorescence recovery. To this aim, the fluorescence intensities of TAMRA aptamer toward various concentrations of UiO-66-$NH_2$ were tested. As illustrated in Fig. 1, the fluorescence intensity of TAMRA aptamer decreased along with UiO-66-$NH_2$ concentration ranging from 0 to 0.35 μg $mL^{-1}$. The maximum fluorescence quenching was obtained when TAMAR aptamer reached 0.2 μg $mL^{-1}$. The fluorescence signal of TAMAR aptamer decreased up to 90%. Consequently, a concentration of 0.2 μg $mL^{-1}$ for UiO-66-$NH_2$ was selected for the subsequent set of experiment.

The binding capacity of TAMRA aptamer on the surface of UiO-66-$NH_2$ was calculated as the following equation [37]:

$$Q = \frac{V \times (C_0 - C_x)}{m} \quad (1)$$

where $Q$ was the adsorption capacity of the TAMRA aptamer, $C_0$ was the concentration of TAMRA aptamer before adsorption, $C_x$ was the concentration of TAMRA aptamer after adsorption, $V$ was the volume of TAMRA aptamer and $m$ was the mass of UiO-66-$NH_2$. The adsorption capacity of TAMRA aptamer increased with increasing the concentration of UiO-66-$NH_2$. When the concentration was up to 0.2 μg $mL^{-1}$, the adsorption capacity began to decrease (Fig. S2). It indicated that the maximum adsorption of TAMRA aptamer on UiO-66-$NH_2$ was 175.34 nmol $mg^{-1}$.

### 3.3. Optimization of experimental conditions

To confirm the sensing platform could be used to detect AFB1, a control experiment with and without AFB1 were conducted. As depicted in Fig. 2A, the fluorescence intensity decreased rapidly when UiO-66-$NH_2$ was added to TAMRA aptamer solution of 37.5 nM (curve a). After incubating with target AFB1, a strong fluorescence emission was recovered which could be attributed to the formation of AFB1/TAMRA aptamer complex. While in the absence of AFB1, the TAMRA aptamer adsorbed on the surface of UiO-66-$NH_2$ and a weak fluorescence emission was measured (curve d). The results illustrated that the fluorescent aptamer sensor work as described previously (section 3.1). Thus, the fluorescence emission was recovered for it obstructed the energy transfer between the fluorescence dye TAMRA and UiO-66-$NH_2$. It worth mentioned that the fluorescence of TAMRA aptamer almost not influenced by AFB1 without UiO-66-$NH_2$ (curve b). The results indicated that the quantity of AFB1 could be analyzed by monitoring the fluorescence signal change.

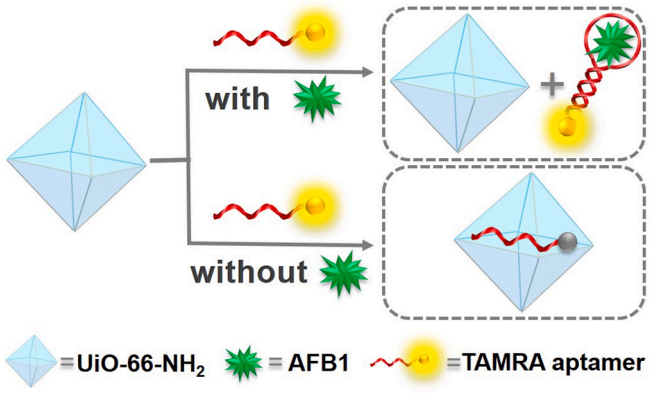


**Scheme 1.** Schematic illustration of the fluorescent aptasensor for AFB1 detection base on UiO-66-$NH_2$.

For better quantification of target, several factors such as the ionic strength and pH of reaction buffer were optimized in the sensing platform. As shown in Fig. S3, introducing 70 ng $mL^{-1}$ AFB1 to the solution of TAMRA aptamer and UiO-66-$NH_2$, the fluorescence intensity increased with increasing the concentration of NaCl. While, the concentration of NaCl higher then 120 mM, the fluorescence intensity decreased. The results could be attributed to the high concentration of $Na^+$ could form weak complexes with aptamer and influenced the conformation of TAMRA aptamer or the target would aggregate which caused lower affinity to TAMRA aptamer [45]. Thus, 120 mM NaCl was choosed in the following experiment. When the pH of Tris-HCl was higher or lower than 7.21, the fluorescence signal recover decreased (Fig. S4). It demonstrated that Tris-HCl (pH 7.21) was a suitable buffer for AFB1 detection in the work. The incubation temperature was also investigated at different temperature ranging from 4 to 37 °C. According to Fig. S5, the fluorescence intensity recover was the highest at 37 °C. In addition, 37 °C was chosen as the incubation temperature. Fig. 2B displayed the fluorescence intensity changes in the presence of AFB1 under different incubation time. The fluorescence intensity enhanced significantly with incubation time consuming and tended to stabilize at 55 min. Thus, 55 min was regarded as the incubation time for AFB1 detection in the sensing platform.

### 3.4. Quantitative detection of AFB1

Under the optimized conditions, we evaluated the sensitivity of the assay for AFB1 detection. Fig. 3A described the typical fluorescence emission spectra of TAMRA aptamer in Tris-HCl buffer, containing different concentrations of target AFB1 upon addition of UiO-66-$NH_2$. The fluorescence intensity gradually enhanced with increasing concentrations of AFB1 from 0 to 180 ng $mL^{-1}$ (Fig. 3B). The results clearly demonstrated that when more AFB1 was added, more TAMRA aptamer changed into internal loop structures and detached from the surface of UiO-66-$NH_2$, resulting in a higher fluorescence enhancement.

Fig. S6 displayed that the fluorescence intensity was proportional to AFB1 concentration from 0 to 0.5 ng $mL^{-1}$ with the square of the correlation coefficient $R^2$ of 0.995. The linear relationship can be described as $F = 25.1444C + 14.87575$. Fig. S7 exhibited that the fluorescence intensity was proportional to AFB1 concentration from 1.5 to 3.0 ng $mL^{-1}$ with the square of the correlation coefficient $R^2$ of 0.992. The linear relationship can be described as $F = 5.96864C + 21.5816$, where $F$ was the fluorescence intensity and $C$ was the concentration of AFB1 (ng.$mL^{-1}$). The limit of detection was calculated as the junction of the two linear range which was 0.35 ng $mL^{-1}$. It was superior or comparable with the previous reports for AFB1 detection (Table 1). Thus, the proposed assay was a simple and straightforward strategy for sensitive detection of AFB1.

### 3.5. Selectivity detection of AFB1

To confirm the selectivity of the sensing platform for AFB1 detection, 210 ng $mL^{-1}$ of other mycotoxins such as ochratoxin A (OTA) and zearalenone (ZEN) were tested under the same experiment conditions as 70 ng $mL^{-1}$ AFB1. The two mycotoxins own similar molecule structure to AFB1. As displayed in Fig. 4A, the AFB1 could be well distinguished from ZEN as well as OTA. The fluorescence intensity toward AFB1 demonstrated 5.35-fold and 5.11-fold higher than ZEN and OTA,

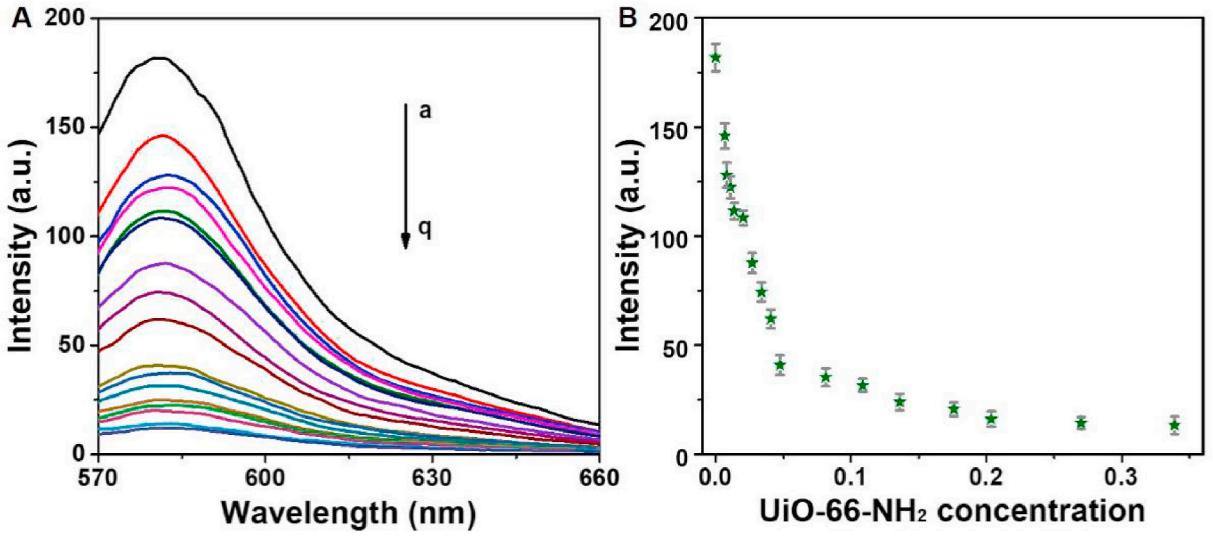


**Fig. 1.** (A) Fluorescence emission spectra and (B) fluorescence intensity of TAMRA aptamer in the presence of different concentration of UiO-66-$NH_2$ (from a to q): 0, $6.79 \times 10^{-3}$, $8.14 \times 10^{-3}$, $10.86 \times 10^{-3}$, $13.60 \times 10^{-3}$, $20.36 \times 10^{-3}$, $27.00 \times 10^{-3}$, $33.9 \times 10^{-3}$, $40.71 \times 10^{-3}$, $47.50 \times 10^{-3}$, $81.40 \times 10^{-3}$, $108.60 \times 10^{-3}$, $136.00 \times 10^{-3}$, $176.00 \times 10^{-3}$, $203.60 \times 10^{-3}$, $270.00 \times 10^{-3}$, $339.00 \times 10^{-3}$ μg $mL^{-1}$. The concentrations of TAMRA aptamer was 35.7 nmol $L^{-1}$. Each data point was the mean of three measurements with error bars; λex/λem = 560/580 nm.

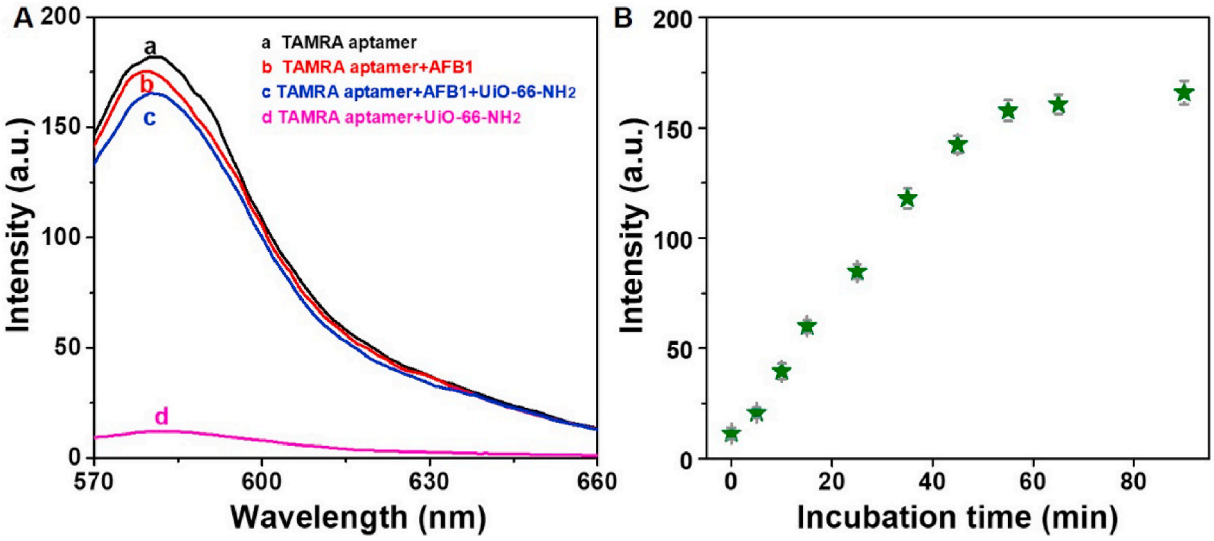


**Fig. 2.** (A) The fluorescence emission of TAMRA aptamer and TAMRA aptamer/UiO-66-$NH_2$ complex with and without AFB1. (B) The fluorescence intensity of TAMRA aptamer/UiO-66-$NH_2$ complex in the presence of AFB1 under different incubation time. The concentrations were TAMRA aptamer = 35.7 nmol $L^{-1}$, UiO-66-$NH_2$ = 0.2 μg $mL^{-1}$ and AFB1 = 180 ng $mL^{-1}$. Each data point was the mean of three measurements with error bars; λex/λem = 560/580 nm.

respectively, due to the specific interaction between TAMRA aptamer and AFB1. Moreover, the mixture of AFB1 and OTA or AFB1 and ZEN was added to the solution of TAMRA aptamer and UiO-66-$NH_2$ in Tris-HCl buffer, the fluorescence intensity was almost unchanged compared to only AFB1 (Fig. 4B). These results confirmed that the assay was high specificity for AFB1 detection over other mycotoxins.

### 3.6. Detection of AFB1 in food samples

To verify the practical applicability and reliability of the sensing platform for AFB1 detection, the recovery experiments were investigated in milk, rice and corn using the standard addition method. The food samples were bought from supermarket, which were pretreated as our previous report [42]. The fluorescence intensity enhanced significantly with increasing the concentrations of AFB1 in these food samples using the proposed assay (Figs. S8–10). The performance of the sensing platform was verified by commercial HPLC. As shown in Table 2, the recoveries in the three kind of food samples were in range of 90.42%–104.14% with the relative standard deviation (RSD) in range of 2.50%–5.60%. These experimental results indicated that the proposed assay holds a great promise for the detection of AFB1 in food samples with favorable reliability.

### 3.7. Mechanism for AFB1 detection

To investigate mechanism of the sensing platform for AFB1 detection, we calculated the quenching constant of TAMRA aptamer and the binding constant of AFB1. The quenching constant was evaluated by Stern-Volmer equation [46]:

$$\frac{F_0}{F} = 1 + K_{SV}[Q] \quad (2)$$

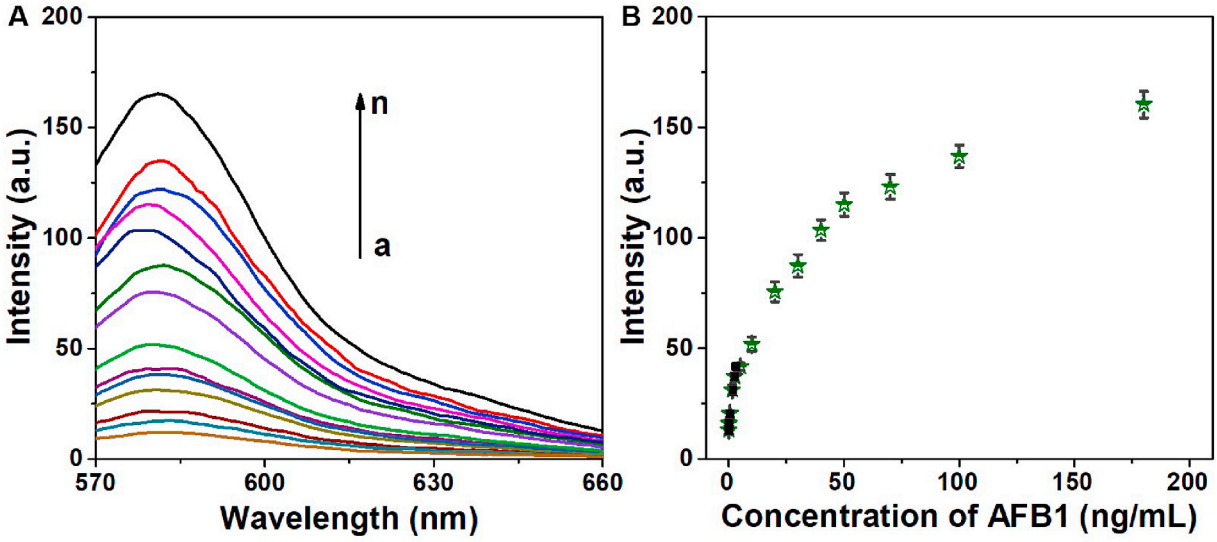


**Fig. 3.** (A) Fluorescence emission spectra of TAMRA aptamer/UiO-66-$NH_2$ complex in the presence of different concentration (from a to n) of AFB1: 0, 0.005, 0.5, 1.5, 2.5, 3, 10, 20, 30, 40, 50, 70, 100, 180 ng $mL^{-1}$. (B) Linear relationship between the fluorescence intensity and AFB1 concentration range (0–180 ng $mL^{-1}$). The concentrations were TAMRA aptamer = 35.7 nmol $L^{-1}$, UiO-66-$NH_2$ = 0.2 μg $mL^{-1}$. Each data point was the mean of three measurements with error bars; λex/λem = 560/580 nm.

**Table 1**
Comparison fluorescence aptasensor for AFB1 detection.

| Analytical Methods | Limit of Detection (ng/mL) | Time (h) | Recognition Probe | Ref |
|---|---|---|---|---|
| FRET-based | 0.91 | <1 | Four labeled | [48] |
| FRET-based | 1.60 | <1 | Dual labeled | [49] |
| QD-aptamer/AuNPs | 1.00 | <1 | Dual labeled | [50] |
| Rh6G/aptamer/MSN-$NH_2$ | 0.13 | 5 | Label-free | [51] |
| AIE/aptamer/GO | 0.25 | 1.5 | Label-free | [42] |
| DNaseI-based | 0.50 | <1 | Single-labeled | [52] |
| TAMRA aptamer/UiO-66-$NH_2$ | 0.35 | <1 | Single-labeled | This work |

where $F_0$ and $F$ was the fluorescence intensity of TAMRA aptamer in the absence and presence of UiO-66-$NH_2$. [Q] was the concentration of UiO-66-$NH_2$. $K$sv was the Stern-Volmer dynamic quenching constant.

Equation (2) was applied to determine the value of $K_{sv}$ by linear regression of a plot of $F_0/F$ against [Q]. As shown in Fig. 5A, the value of $K_{sv}$ decreased with increasing the reaction temperature (Table S1). It illustrated that the quenching mechanism of TAMRA aptamer in presence of UiO-66-$NH_2$ was static quenching. Thus the binding constant for AFB1 using the sensing platform could be determined using the following equation [47]:

$$\log\frac{F_0 - F}{F} = \log K_a + n\log[Q] \quad (3)$$

where $K_a$ was the binding constant. From equation (3), the values $K_a$ at 310 K were observed. Fig. 5B displayed the linear regression of a plot of

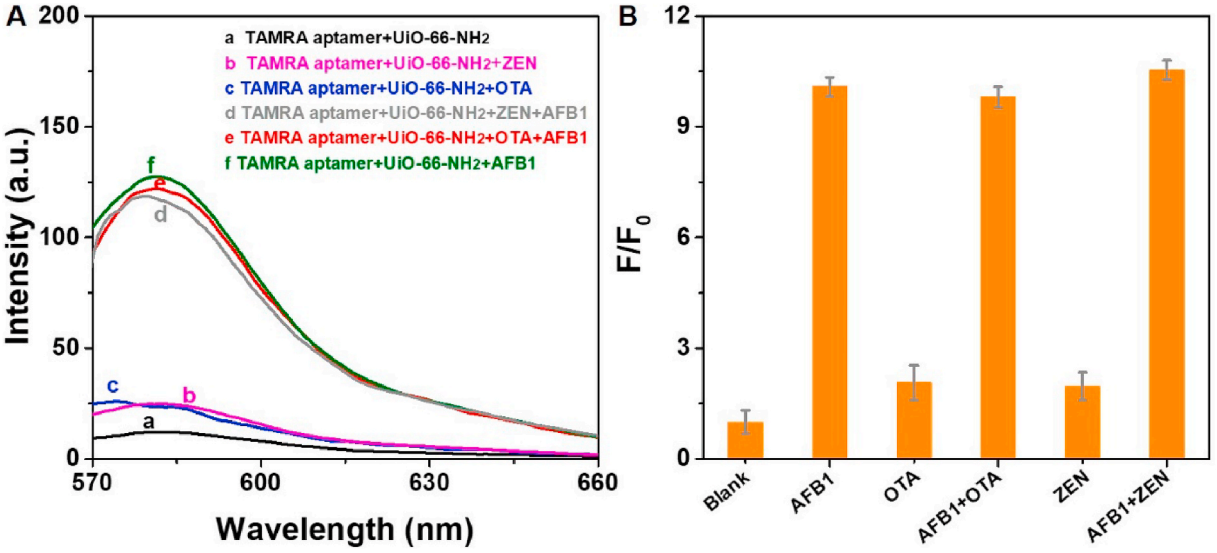


**Fig. 4.** The fluorescence emission spectra (A) and selectivity (B) of the sensing platform in the presence of different mycotoxins. $F$ and $F_0$ represented the fluorescence intensity of TAMRA aptamer/UiO-66-$NH_2$ complex with and without mycotoxins. Concentrations were TAMRA aptamer = 35.7 nmol $L^{-1}$, UiO-66-$NH_2$ = 0.2 μg $mL^{-1}$, AFB1 = 70 ng $mL^{-1}$, OTA = 210 ng $mL^{-1}$, ZEN = 210 ng $mL^{-1}$. Each data point was the mean of three measurements with error bars; λex/λem = 560/580 nm.

**Table 2**
Detection of AFB1 in food samples using the designed sensing platform.

| Sample | Added (ng/mL) | HPLC measured mean[a]±SD[b] (ng/mL) | Proposed method mean[a]±SD[b] (ng/mL) | Recovery (%) |
|---|---|---|---|---|
| Milk | 0.00 | n[c] | n[c] | / |
| | 1.52 | 1.39 ± 0.06 | 1.58 ± 0.03 | 104.14 |
| | 2.84 | 2.63 ± 0.07 | 2.93 ± 0.06 | 103.10 |
| Corn | 0.00 | n[c] | n[c] | / |
| | 1.52 | 1.43 ± 0.038 | 1.47 ± 0.03 | 96.38 |
| | 2.84 | 2.68 ± 0.05 | 2.77 ± 0.03 | 97.36 |
| Rice | 0.00 | n[c] | n[c] | / |
| | 1.52 | 1.42 ± 0.04 | 1.43 ± 0.03 | 94.21 |
| | 2.84 | 2.75 ± 0.05 | 2.57 ± 0.05 | 90.42 |

[a] The mean of three determinations.
[b] SD = standard deviation.
[c] No AFB1 concentration was detected.

$\log\frac{F_0-F}{F}$ against log[Q]. The values $K_a$ were obtained to be 23.882 and 5.389 in the absence and presence of AFB1 (Table S2). The results demonstrated that the adsorption affinity of TAMRA aptamer and UiO-66-$NH_2$ decreased after introducing AFB1 to the sensing platform. Therefore, the fluorescence intensity of TAMRA aptamer recovered.

To confirm the different affinities of TAMRA aptamer and UiO-66-$NH_2$ in the absence and presence of AFB1, agrose gel electrophoresis was carried out (Fig. S9). Under UV excitation, TAMRA aptamer displayed one light band (lane 2). While, no band was observed after TAMRA aptamer incubated with UiO-66-$NH_2$ (lane 3), suggesting that TAMRA aptamer was adsorbed on the surface of UiO-66-$NH_2$, the TAMRA aptamer/UiO-66-$NH_2$ complex possessed larger molecular weight and moved slower. In the presence of AFB1, the TAMRA aptamer binded to AFB1 and detached from the UiO-66-$NH_2$ surface. Thus, there was a light band (lane 5).

To further illustrate the mechanism for AFB1 detection in the sensing platform, UV–vis spectrum was perfomed. As shown in Fig. 6A, there was a DNA characteristic absorption at 260 nm in the TAMRA aptamer adsorption spectrum (curve a). Adding UiO-66-$NH_2$ to the solution of TAMRA aptamer, the DNA characteristic absorption at 260 nm decreased (curve c), suggesting that TAMRA aptamer was adsorbed on the surface of UiO-66-$NH_2$. While, introducing AFB1 to the solution of TAMRA aptamer and UiO-66-$NH_2$, the DNA characteristic absorption significantly enhanced (curve b), indicating that TAMRA aptamer binded to AFB1 and detached from the surface of UiO-66-$NH_2$. To better understand the mechanism for AFB1 detection in the sensing platform, particle size analysis was measured. As exhibited in Fig. 6B, the individual particle sizes of TAMRA aptamer/AFB1 and UiO-66-$NH_2$ were 100.15 nm (curve a) and 315.75 nm (curve b). Adding TAMRA aptamer to the solution of UiO-66-$NH_2$, the individual particle size increased to 516.02 nm (curve d). The result demonstrated that the TAMRA aptamer adsorbed on the surface of UiO-66-$NH_2$ and formed a large size class. While, introducing AFB1 the solution of TAMRA aptamer/UiO-66-$NH_2$, the individual particle size decreased to 397.16 nm (curve c). The results illustrated that the TAMRA aptamer changed into internal loop structure and detached from the surface of UiO-66-$NH_2$ after adding AFB1 to the sensing platform.

## 4. Conclusions

In the research, we had constructed a fluorescent aptasensor for determination of AFB1 using TAMRA aptamer and UiO-66-$NH_2$. The fluorescence emission of TAMRA aptamer was effectively quenched by UiO-66-$NH_2$, while it could be recovered with AFB1 presence for its specifically bind to AFB1 with high affinity and selectivity. Using the sensing platform, 0.35 ng $mL^{-1}$ AFB1 could be analyzed. It exhibited excellent selectivity against other common mycotoxins. Furthermore, it was successfully employed to food samples such as rice, mile and corn with satisfied results. The sensing platform offered a simple, low cost, sensitive and selective assay for various targets analysis with broad application in the field of food safety.

## Declaration of competing interest

We guarantee the subject matter is original, and has not been previously published and is not have and being submitted elsewhere.

## Credit authorship contribution state

Yongmei Jia: Analyzed the data, Resources, Writing-original draft, Writing-review & editing, Funding acquisition. Guohua Zhou: Investigation, Discussed the results. Xudong Wang: Data curation, Formal analysis, Discussed the results. Yingzi Zhang: Software. Zhiguo Li: Data

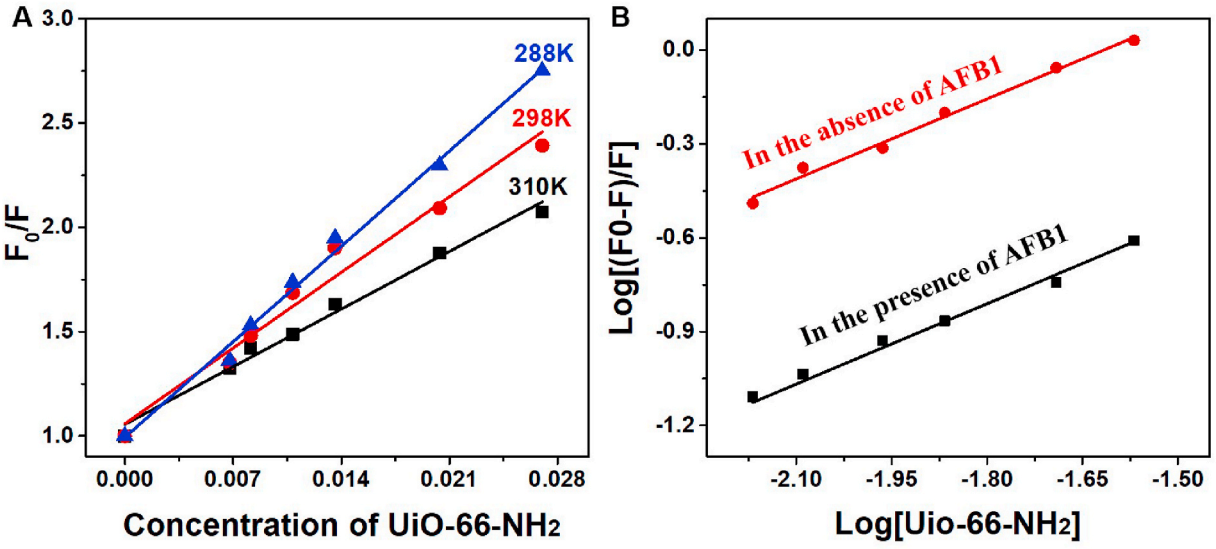


**Fig. 5.** (A) Stern-Volmer plots describing TAMRA aptamer quenching caused by UiO-66-$NH_2$ at different temperature. (B) The results of binding constant *K* in the presence and absence of AFB1 in the sensing platform. Concentrations were TAMRA aptamer = 35.7 nmol $L^{-1}$, AFB1 = 180 ng $mL^{-1}$, UiO-66-$NH_2$ = 0.00, 6.79 × $10^{-3}$, 8.14 × $10^{-3}$, 10.86 × $10^{-3}$, 13.60 × $10^{-3}$, 20.36 × $10^{-3}$, 27.00 × $10^{-3}$ μg $mL^{-1}$. Each data point was the mean of three measurements with error bars; λex/λem = 560/580 nm.

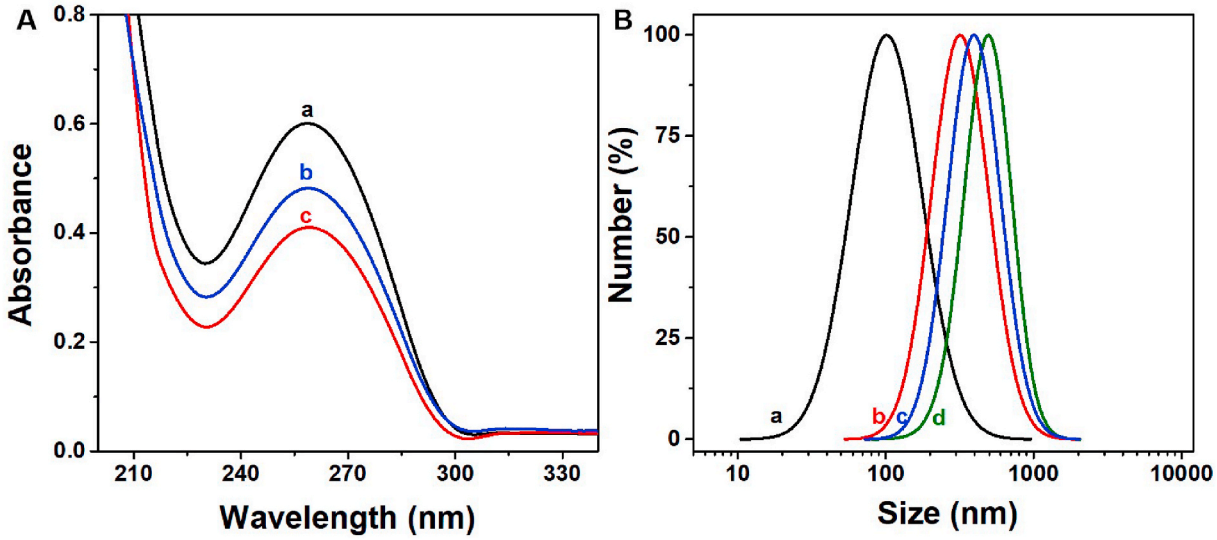


**Fig. 6.** (A) The UV–vis absorption spectroscopy of the TAMRA aptamer/UiO-66-$NH_2$ sensing platform. a: TAMRA aptamer; b: UiO-66-$NH_2$/TAMRA aptamer/AFB1; c: UiO-66-$NH_2$/TAMRA aptamer. (B) The particle size analysis of the TAMRA aptamer/UiO-66-$NH_2$ sensing platform. a: TAMRA aptamer/AFB1; b: UiO-66-$NH_2$; c: UiO-66-$NH_2$/TAMRA aptamer/AFB1; d: UiO-66-$NH_2$/TAMRA aptamer. Concentrations were TAMRA aptamer = 0.7 mmol $L^{-1}$, AFB1 = 3 μg $mL^{-1}$, UiO-66-$NH_2$ = 2.625 μg $mL^{-1}$. Each data point was the mean of three measurements with error bars; λex/λem = 560/580 nm.

curation, Project administration. Peilian Liu: Formal analysis, Project administration. Biao Yu: Formal analysis, Supervision. Jun Zhang: Project administration, Supervision.

## Declaration of competing interest

We guarantee the subject matter is original, and has not been previously published and is not have and being submitted elsewhere.

## Acknowledgements

We gratefully acknowledge the support of the National Natural Science Foundation of China (21705071, 21605074, 21805125, 61674073), the Natural Science Foundation of Guangdong province of China (2016A030310362, 2014A030310274, 2018A030313101, 2018A030307071), the Initiatory Financial Support from Lingnan Normal University (ZL1611, ZL1404), Young Talent of Lingnan Normal University, Science and Technology Planning Project of Guangdong Province (2017A050506056), the Research Group of Rare Earth Resource Exploiting and Luminescent Materials (2017KCXTD022).

## Appendix A. Supplementary data

Supplementary data to this article can be found online at https://doi.org/10.1016/j.talanta.2020.121342.

## References

[1] H.L. Xie, X.P. Wang, L.X. Zhang, T. Wang, W. Zhang, J. Jiang, P.K. Chang, Z. Y. Chen, D. Bhatnagar, Q. Zhang, P.W. Li, Monitoring metabolite production of aflatoxin biosynthesis by orbitrap fusion mass spectrometry and a D-optimal mixture design method, Anal. Chem. 90 (2018) 14331–14338.
[2] F.Y. Wang, Y.M. Han, S.M. Wang, Z.J. Ye, L. Wei, L.H. Xiao, Single-particle LRET aptasensor for the sensitive detection of aflatoxin B1 with upconversion nanoparticles, Anal. Chem. 91 (2019) 11856–11863.
[3] E.J. Jo, J.Y. Byun, H. Mun, D. Bang, J.H. Son, J.Y. Lee, L.P. Lee, M.G. Kim, Single-step LRET aptasensor for rapid mycotoxin detection, Anal. Chem. 90 (2018) 716–722.
[4] L. Wu, F. Ding, W.M. Yin, J. Ma, B.R. Wang, A. Nie, H.Y. Han, From electrochemistry to electroluminescence: development and application in a ratiometric aptasensor for aflatoxin B1, Anal. Chem. 89 (2017) 7578–7585.
[5] M. Sun, D. Xu, S. Wang, K. Uchiyama, Inkjet-based dispersive liquid-liquid microextraction method coupled with UHPLC-MS/MS for the determination of aflatoxins in wheat, Anal. Chem. 91 (2019) 3027–3034.
[6] H.M. Liu, A.X. Lu, H.L. Fu, B.R. Li, M.H. Yang, J.H. Wang, Y.X. Luan, Affinity capture of aflatoxin B1 and B2 by aptamer-functionalized magnetic agarose microspheres prior to their determination by HPLC, Microchim. Acta 185 (2018) 326.
[7] B. Wang, J.S. Zheng, A.L. Ding, L.Q. Xu, J.C. Chen, C.M. Li, Highly sensitive aflatoxin B1 sensor based on DNA-guided assembly of fluorescent probe and TdT-assisted DNA polymerization, Food Chem. 294 (2019) 19–26.
[8] X.S. Yang, D.M. Shi, S.M. Zhu, B.J. Wang, X.J. Zhang, G.F. Wang, Portable aptasensor of aflatoxin B1 in bread based on a personal glucose meter and DNA walking machine, ACS Sens. 3 (2018) 1368–1375.
[9] L. Xu, H.Q. Zhang, X.W. Yan, H.Y. Peng, Z.X. Wang, Q. Zhang, P.W. Li, Z.W. Zhang, X.C. Le, Binding-induced DNA dissociation assay for small molecules: sensing aflatoxin B1, ACS Sens. 3 (2018) 2590–2596.
[10] X. Li, L. Yang, C. Men, Y.F. Xie, J.J. Liu, H.Y. Zou, Y.F. Li, L. Zhan, C.Z. Huang, Photothermal soft nanoballs developed by loading plasmonic $Cu_2$-xSe nanocrystals into liposomes for photothermal immunoassay of aflatoxin B1, Anal. Chem. 91 (2019) 4444–4450.
[11] L.Z. Chen, J. Chao, X.M. Qu, H.B. Zhang, D. Zhu, S. Su, A. Aldalbahi, L.H. Wang, H. Pei, Probing cellular molecules with polyA-based engineered aptamer nanobeacon, ACS Appl. Mater. Interfaces 9 (2017) 8014–8020.
[12] G. Bayramoglu, C. Ozalp, M. Oztekin, U. Guler, B. Salih, M.Y. Arica, Design of an aptamer-based magnetic adsorbent and biosensor systems for selective and sensitive separation and detection of thrombin, Talanta 191 (2019) 59–66.
[13] B.A. Borsa, B.G. Tuna, F.J. Hernandez, L.I. Hernandez, G. Bayramoglu, M.Y. Arica, V.C. Ozalp, Staphylococcus aureus detection in blood samples by silica nanoparticle-oligonucleotides conjugates, Biosens. Bioelectron. 86 (2016) 27–32.
[14] G. Bayramoglu, V.C. Ozalp, M. Oztekin, M.Y. Arica, Rapid and label-free detection of Brucella melitensis in milk and milk products using an aptasensor, Talanta 200 (2019) 263–271.
[15] Y.P. Li, Q. Zhao, Aptamer structure switch fluorescence anisotropy assay for small molecules using streptavidin as an effective signal amplifier based on proximity effect, Anal. Chem. 91 (2019) 7379–7384.
[16] Y.N. Li, J.Y. Wang, B. Zhang, Y. He, J.P. Wang, S. Wang, A rapid fluorometric method for determination of aflatoxin B1 in plant-derived food by using a thioflavin T-based aptasensor, Microchim. Acta 186 (2019) 214.
[17] V.K. Gupta, N. Mergu, L.K. Kumawat, A.K. Singh, Selective naked-eye detection of Magnesium (II) ions using a coumarin-derived fluorescent probe, Sensor. Actuator. B Chem. 207 (2015) 216–223.
[18] R.N. Goyal, V.K. Gupta, A. Sangal, N. Bachheti, Voltammetric determination of uric acid at a fullerene-C60-modified glassy carbon electrode, Electroanalysis 17 (2005) 2217–2223.
[19] N. Hao, J.W. Lu, Z. Zhou, R. Hua, K. Wang, A pH-resolved colorimetric biosensor for simultaneous multiple target detection, ACS Sens. 3 (2018) 2159–2165.
[20] X. Li, F. Yang, J.X.H. Wong, H.Z. Yu, Integrated smartphone-app-chip system for on-site parts-per-billion-level colorimetric quantitation of aflatoxins, Anal. Chem. 89 (2017) 8908–8916.
[21] J.H. Wu, L.W. Zeng, N.L. Li, C.S. Liu, J.H. Chen, A wash-free and label-free colorimetric biosensor for naked-eye detection of aflatoxin B1 using G-quadruplex as the signal reporter, Food Chem. 298 (2019) 125034.
[22] V.K. Gupta, N. Mergu, L.K. Kumawat, A.K. Singh, Selective naked-eye detection of magnesium (II) ions using a coumarin-derived fluorescent probe, Sensor. Actuator. B Chem. 207 (2015) 216–223.

[23] J.J. Ge, Y. Zhao, C.L. Li, G.F. Jie, Versatile Electrochemiluminescence and electrochemical "On-Off" assays of methyltransferases and aflatoxin B1 based on a novel multifunctional DNA nanotube, Anal. Chem. 91 (2019) 3546–3554.
[24] G. Peng, X.Y. Li, F. Cui, Q.Y. Qiu, X.J. Chen, H. Huang, Aflatoxin B1 electrochemical aptasensor based on tetrahedral DNA nanostructures functionalized three dimensionally ordered macroporous $MoS_2$-AuNPs film, ACS Appl. Mater. Interfaces 10 (2018) 17551–17559.
[25] Y.X. Lin, Q. Zhou, D.P. Tang, Dopamine-loaded liposomes for in-situ amplified photoelectrochemical immunoassay of AFB1 to enhance photocurrent of $Mn^{2+}$-doped $Zn_3(OH)_2V_2O_7$ nanobelts, Anal. Chem. 89 (2017) 11803–11810.
[26] M.L. Yola, V.K. Gupta, T. Eren, A.E. Şen, N. Atar, A novel electro analytical nanosensor based on graphene oxide/silver nanoparticles for simultaneous determination of quercetin and morin, Electrochim. Acta 120 (2014) 204–211.
[27] H.K. Maleh, F.T. Javazmi, N. Atar, M.L. Yola, V.K. Gupta, A.A. Ensafi, A novel DNA biosensor based on a pencil graphite electrode modified with polypyrrole/functionalized multiwalled carbon nanotubes for determination of 6-mercaptopurine anticancer drug, Ind. Eng. Chem. Res. 54 (2015) 3634–3639.
[28] F.J. Zheng, W. Ke, L.X. Shi, H. Liu, Y. Zhao, Plasmonic Au-Ag janus nanoparticle engineered ratiometric surface-enhanced Raman scattering aptasensor for ochratoxin A detection, Anal. Chem. 91 (2019) 11812–11820.
[29] Y.M. Jia, G.H. Zhou, P.L. Liu, Z.G. Li, B. Yu, Recent development of aptamer sensors for the quantification of aflatoxin B1, Appl. Sci. Basel 9 (2019) 2364.
[30] R. Liu, W. Li, T.T. Cai, Y. Deng, Z. Ding, Y. Liu, X.R. Zhu, X. Wang, J. Liu, B. W. Liang, T.S. Zheng, J.L. Li, $TiO_2$ Nanolayer-enhanced fluorescence for simultaneous multiplex mycotoxin detection by aptamer microarrays on a porous silicon surface, ACS Appl. Mater. Interfaces 10 (2018) 14447–14453.
[31] Z.B. Li, N. Xue, H.Y. Ma, Z.Y. Cheng, X.M. Miao, An ultrasensitive and switch-on platform for aflatoxin B1 detection in peanut based on the fluorescence quenching of graphene oxide-gold nanocomposites, Talanta 181 (2018) 346–351.
[32] S. Niazi, I.M. Khan, Y. Yu, I. Pasha, M. Shoaib, A. Mohsin, B.S. Mushtaq, W. Akhtar, Z. Wang, A "turn-on" aptasensor for simultaneous and time-resolved fluorometric determination of zearalenone, trichothecenes A and aflatoxin B1 using WS2 as a quencher, Microchim. Acta 186 (2019) 575.
[33] M.L. Guo, Q. Hou, G.I.N. Waterhouse, J.Y. Hou, S.Y. Ai, X.Y. Li, A simple aptamer-based fluorescent aflatoxin B1 sensor using humic acid as quencher, Talanta 205 (2019) 120131.
[34] B. Wang, Y.F. Chen, Y.Y. Wu, B. Weng, Y.S. Liu, Z.S. Lu, C.M. Li, C. Yu, Aptamer induced assembly of fluorescent nitrogen-doped carbon dots on gold nanoparticles for sensitive detection of AFB1, Biosens. Bioelectron. 78 (2016) 23–30.
[35] H.Q. Zhao, G.H. Qiu, Z. Liang, M.M. Li, B. Sun, L. Qin, S.P. Yang, W.H. Chen, J. X. Chen, A zinc(II)-based two-dimensional MOF for sensitive and selective sensing of HIV-1 ds-DNA sequences, Anal. Chim. Acta 922 (2016) 55–63.
[36] H.S. Wang, H.L. Liu, K. Wang, Y. Ding, J.J. Xu, X.H. Xia, H.Y. Chen, Insight into the unique fluorescence quenching property of metal-organic frameworks upon DNA binding, Anal. Chem. 89 (2017) 11366–11371.
[37] Y.T. Liang, J. He, Z.P. Huang, H.Y. Li, Y.X. Zhang, H.G. Wang, C.F. Rui, Y.Y. Li, L. Q. You, K. Li, S.S. Zhang, An amino functionalized zirconium based metal organic framework of type UiO-66-$NH_2$ covered with a molecularly imprinted polymer as a sorbent for the extraction of aflatoxins AFB1, AFB2, AFG1 and AFG2 from grain, Microchim. Acta 187 (2020) 32.
[38] J.S. Kahn, L. Freage, N. Enkin, M.A.A. Garcia, I. Willner, Stimuli responsive DNA functionalized metal-organic frameworks (MOFs), Adv. Mater. 29 (2017) 1602782.
[39] H.M. Meng, X.X. Hu, G.Z. Kong, C. Yang, T. Fu, Z.H. Li, X.B. Zhang, Aptamer-functionalized nanoscale metal-organic frameworks for targeted photodynamic therapy, Theranostics 8 (2018) 4332–4344.
[40] L.L. Wu, Z. Wang, S.N. Zhao, X. Meng, X.Z. Song, J. Feng, S.Y. Song, H.J. Zhang, A metal-organic framework/DNA hybrid system as a novel fluorescent biosensor for mercury(II) ion detection, Chem. Eur J. 22 (2016) 477–480.
[41] H.L. Tan, G.G. Tang, Z.X. Wang, Q. Li, J. Gao, S.M. Wu, Magnetic porous carbon nanocomposites derived from metal-organic frameworks as a sensing platform for DNA fluorescent detection, Anal. Chim. Acta 940 (2016) 136–142.
[42] Y.M. Jia, F. Wu, P.L. Liu, G.H. Zhou, B. Yu, X.D. Lou, F. Xia, A label-free fluorescent aptasensor for the detection of Aflatoxin B1 in food samples using AIEgens and graphene oxide, Talanta 198 (2019) 71–77.
[43] P.P. Hu, N. Liu, K.Y. Wu, L.Y. Zhai, B.P. Xie, B. Sun, W.J. Duan, W.H. Zhang, J. X. Chen, Successive and specific detection of $Hg^{2+}$ and $I^-$ by a DNA@MOF biosensor: experimental and simulation studies, Inorg. Chem. 57 (2018) 8382–8389.
[44] H.S. Wang, J. Li, J.Y. Li, K. Wang, Y. Ding, X.H. Xia, Lanthanide-based metal-organic framework nanosheets with unique fluorescence quenching properties for two-color intracellular adenosine imaging in living cells, NPG Asia Mater. 9 (2017), 354-354.
[45] T. Hianik, V. Ostatnás, M. Sonlajtnerova, I. Grman, Influence of ionic strength, pH and aptamer configuration for binding affinity to thrombin, Bioelectrochemistry 70 (2007) 127–133.
[46] Y. Wei, J.Q. Li, C. Dong, S.M. Shuang, D.S. Liu, C.W. Huie, Investigation of the association behaviors between biliverdin and bovine serum albumin by fluorescence spectroscopy, Talanta 70 (2006) 377–382.
[47] G. Zhang, N. Zhao, X. Hu, J. Tian, Interaction of alpinetin with bovine serum albumin: probing of the mechanism and binding site by spectroscopic methods, Spectrochim. Acta, Part A 76 (2010) 410–417.
[48] X.H. Xia, Y.X. Wang, H. Yang, Y. Dong, K.X. Zhang, Y.H. Lu, R.J. Deng, Q. He, Enzyme-free amplified and ultrafast detection of aflatoxin B1 using dual-terminal proximity aptamer probes, Food Chem. 283 (2019) 32–38.
[49] L. Chen, F. Wen, M. Li, X.D. Guo, S.L. Li, N. Zheng, J.Q. Wang, A simple aptamer-based fluorescent assay for the detection of aflatoxin B1 in infant rice cereal, Food Chem. 215 (2017) 377–382.
[50] F.S. Sabet, M. Hosseini, H. Khabbaz, M. Dadmehr, M.R. Ganjali, FRET-based aptamer biosensor for selective and sensitive detection of aflatoxin B1 in peanut and rice, Food Chem. 220 (2017) 527–532.
[51] H.X. Tan, L. Ma, T. Guo, H.Y. Zhou, L. Chen, Y.H. Zhang, H.J. Dai, Y. Yu, A novel fluorescence aptasensor based on mesoporous silica nanoparticles for selective and sensitive detection of aflatoxin B1, Anal. Chim. Acta 1068 (2019) 87–95.
[52] J.J. Zhang, Z.M. Li, S.C. Zhao, Y. Lu, Size-dependent modulation of graphene oxide-aptamer interactions for an amplified fluorescence-based detection of aflatoxin B1 with a tunable dynamic range, Analyst 141 (2016) 4029–4034.